

Research papers

Are unexpected chloride ions in molten salt really harmful to stainless steel?



Qi Gao, Yuanwei Lu*, Yanchun Yang, Yuting Wu, Cancan Zhang, Zhansheng Fan

MOE Key Laboratory of Enhanced Heat Transfer and Energy Conservation, Beijing Key Laboratory of Heat Transfer and Energy Conversion, Beijing University of Technology, Beijing 100124, China

ARTICLE INFO

Keywords:
Corrosion
Thermal energy storage
Molten salt
Stainless steel

ABSTRACT

Commercial mixed salt generally contains the impurity chloride ion (Cl^-) due to the influence of the preparation process of the single component salt that constitutes the mixed salt. The impurity Cl^- can increase the corrosion of molten salt to metal materials. In order to investigate the effect of molten salt with different content of Cl^- on the corrosion of metal materials, a low melting point quaternary nitrate and solar salt were selected as the base salt to analyze the corrosion rule of Cl^- . Using the weight loss method, the corrosion behaviors of the two molten nitrate salts with and without Cl^- to 316L stainless steel were studied. The results of the corrosion test for 1000 h show that the quaternary mixed molten salt with low Cl^- content of 0.03 wt% has the lowest corrosion rate on 316L stainless steel than that of the other two salts with Cl^- content of 0.01 and 0.05 wt% for the existence of calcium nitrate. Calcium ions (Ca^{2+}) are introduced to solar salt with the same Cl^- content of 0.03 wt% to confirm its corrosion effect on stainless steel. The results show that the addition of a small amount of Cl^- and Ca^{2+} can reduce the corrosion rate of solar salt on 316L stainless steel. The corrosion products morphology analysis by SEM, EDS, and XRD test show that the calcium rich oxide layers containing CaFeO_4 was found in the corrosion layer of stainless steel, which inhibits the further corrosion of stainless steel in molten salt. This finding has the far-reaching implications for inhibiting corrosion of molten salt with Cl^- on stainless steel.

1. Introduction

In order to cope with global warming, countries around the world have adopted “carbon peaks” and “carbon neutralization” as national strategies. Under the guidance of the “double carbon” goal, renewable energy will be developed on a large scale in the future in China. Concentrated Solar Power (CSP) is a promising technology in the field of renewable energy, because the combination of large-scale thermal energy storage (TES) and CSP technology can perfectly solve the problem of discontinuity and instability in solar energy utilization process [1]. Molten salt is an ideal medium for heat transfer and thermal energy storage, which has many advantages, such as wide operating temperature range, high thermal stability, large heat capacity, low cost, low viscosity and so on [2].

The corrosivity of molten salt to metal materials is a very important issue for it affects the safety and reliability of TES system [3], so it has been a research focus recently. At present, CSP plants generally choose the energy storage materials with low corrosivity, such as solar salt, which is composed of 60 wt% sodium nitrate and 40 wt% potassium

nitrate. Some scholars have studied the corrosion behavior of metal materials with solar salt. For example, Xiao et al. studied the corrosion behavior of three stainless steel samples in solar salt and found that the main component of the oxide scale in corrosion layer is iron oxide [4]. Kruizenga et al. studied the corrosion behavior of three stainless steels (stainless steels 316, 347 and 321) in solar salt, and the results show that the oxide scale formed by the reaction between stainless steel and molten salt are mainly composed of FeCr_2O_4 and Fe_3O_4 at high temperature [5]. In addition, Gomes et al. studied the corrosion behavior of 316L and 321H in solar salt and confirmed that FeCr_2O_4 is a stable spinel structure with better protection than Fe_3O_4 and Fe_2O_3 [6]. In a word, the protective oxide scales are generated on the surface of the metal material after contacting with the solar salt, which makes the solar salt have less corrosivity to the metal material.

In general, commercial solar salt is a kind of mixed molten salt constituted of single component nitrate (40 wt% KNO_3 + 60 wt% NaNO_3). The nitrate inevitably contains impurity chloride ions (Cl^-) for its preparation process. The existence of Cl^- is considered to increase the corrosivity of molten salt to metal material. So, in order to ensure the safe operation of CSP plant, the relevant departments of China have

* Corresponding author.

E-mail address: luyuanwei@bjut.edu.cn (Y. Lu).

Nomenclature

| | |
|-----|--------------------------------------|
| CSP | Concentrated Solar Power |
| SEM | Scanning Electron Microscopy |
| XRD | X-ray powder diffraction |
| TES | Thermal Energy Storage |
| EDS | Energy Dispersive X-ray Spectroscopy |

formulated a national standard for the use of molten salt (GB/T. 36376) [7]. Nitrate is divided into 3 grades according to the content of Cl^- , i.e. superior grade, first grade and qualified product, in which the content of Cl^- is 0.01, 0.03 and 0.05 wt%, respectively (as shown in Table 1). For different grades of nitrate, the lower the chlorine content, the higher the production cost.

Many researchers have explored the influence of Cl^- on the corrosivity of molten salt by adding different content of Cl^- to solar salt (analytical pure). For example, the corrosion behavior of carbon steel with different contents of Cl^- (1.2 wt% and 3 wt%) in solar salt has been studied [8]. The results show that Cl^- leads to the lack of adhesion between metal and oxide layer, and the corrosion products crack internally. Moreover, the authors found that the increase of chlorine content resulted in delamination and porosity of the iron oxide layer. As a result, the alloy cannot form a dense protective layer, thus accelerating the corrosion of carbon steel. Federsel et al. [9] found that adding 0.25 wt% Cl^- in solar salt can increase the weight loss of carbon steel, and iron chloride can be formed in the oxide layer. Because iron chloride has high volatility, which makes the oxide layer permanently exfoliate.

However, the above research on the influence of Cl^- on the corrosivity of molten salt with the higher Cl^- content, which is far exceed the Cl^- content specified in the national standard of China. Meantime, there is no relevant report on the effect of low Cl^- content (from 0.01 wt% to 0.05 wt%) on the corrosivity of molten salt. Therefore, it is of great significance to evaluate the corrosion performance of metal material in molten salt with low Cl^- content.

At present, the maximum operating temperature of the existing solar salt is 568 °C, which limits the further increase of the inlet steam temperature of the turbine, for the efficiency of the CSP plant is mainly affected by the inlet steam temperature of the turbine. Therefore it is necessary to increase the decomposition temperature of molten salt and reduce its melting temperature to further broaden operating temperature range of it. Our research group has developed a quaternary mixed molten salt with a melting point of 83.1 °C and a decomposition temperature of 628.5 °C, which can be used as high heat storage medium and its low melting temperature can prevent pipe freezing and blocking in case of accident [10].

The quaternary mixed molten salt with different Cl^- content (0.01 wt%, 0.03 wt% and 0.05 wt%) were used to explore the effect of impurity Cl^- on the corrosivity of the molten salts. After 1000 h of corrosion test, it was found that the corrosion rate of 316L stainless steel in quaternary mixed molten salt with Cl^- content of 0.03 wt% is the lowest for the existence of calcium nitrate. To verify this finding, calcium ions are introduced to solar salt with the same content of Cl^- to confirm its corrosion effect on stainless steel. The corrosion behaviors of 316L

stainless steel in two molten nitrate salts with and without Cl^- were analyzed and the corrosion inhibition process was discussed.

2. Experimental

2.1. Preparation of mixed molten salt and stainless steel sample

(1) Preparation of mixed molten salt. The materials used in this experiment include $\text{Ca}(\text{NO}_3)_2 \cdot 4\text{H}_2\text{O}$, KNO_3 , NaNO_3 , NaNO_2 and KCl , which are all produced by Beijing Tongguang Fine Chemical Co., Ltd. And the purity of these materials is ≥99.9 %. In the experiment, KCl was used to change the content of Cl^- in molten salt [11].

Firstly, the quaternary mixed molten salt (16.67 wt% $\text{Ca}(\text{NO}_3)_2 \cdot 4\text{H}_2\text{O} + 44.17$ wt% $\text{KNO}_3 + 5.83$ wt% $\text{NaNO}_3 + 33.33$ wt% NaNO_2) and solar salt (40 wt% $\text{KNO}_3 + 60$ wt% NaNO_3) were selected as the base salt, and they were weighed in a certain proportion, respectively. Then, different amounts of KCl were added to the quaternary mixed molten salt to prepare quaternary mixed molten salt with Cl^- content of 0.01 wt%, 0.03 wt% and 0.05 wt% respectively.

Similarly, KCl was added to solar salt to prepare solar salt with Cl^- content of 0.03 wt%. Also, $\text{Ca}(\text{NO}_3)_2 \cdot 4\text{H}_2\text{O}$ (1 wt%) was added to the solar salt with Cl^- content of 0.03 wt% to prepare solar salt with additive (Cl^- and Ca^{2+}). In addition, all the molten salt samples were placed in a drying oven and dried at 150 °C for 48 h before being mixed. Finally, the mixed molten salts were mixed by static melting in the muffle furnace at 300 °C for >12 h.

(2) Preparation of stainless steel sample. The sample size of 316L stainless steel is 40 mm × 25 mm × 2 mm, and the ingredient of the 316L stainless steel is listed in Table 2. Firstly, the surface of the sample was polished with silicon carbide (SiC) P1000 abrasive paper. Secondly, these samples were degreased with ethanol and cleaned with deionized water. Finally, the stainless steel samples were dried in the dry oven, and the size and initial mass m_i of these samples were recorded.

2.2. Experimental methods and process

The static corrosion experiments of 316L stainless steel samples were carried out by weight loss method. 316L stainless steel samples were placed vertically in different corundum crucibles containing different molten salt. In order to avoid experimental contingency, three identical stainless steel samples were placed in each corundum crucible. Finally, the corundum crucibles were placed in a muffle furnace and kept at a constant temperature of 565 °C for 1000 h in air atmosphere. After reaching the corrosion time, the stainless steel samples were taken from the muffle furnace and cooled to room temperature. The corroded samples were treated according to the American Society for Testing and Materials (ASTM) standard G1-03 (2017). Firstly, the samples were washed with deionized water and cleaned with a soft brush to remove the molten salt from its surface. Secondly, the samples were washed and dried in the ethanol solution, after which they were placed in 1.5 mol/L nitric acid solution at 70 °C for 300 min to remove the surface corrosion layer. Lastly, the processed samples were washed with deionized water and then dried. After the above steps are completed, the final mass m_f of the sample at each corrosion time is recorded. Eq. (1) can be used to obtain the mass loss of the sample.

$$\frac{\Delta m}{A_0} = \frac{m_i - m_f}{A_0} \quad (1)$$

where Δm is the sample mass loss (mg), m_i is the initial mass of the sample (mg), m_f is the final mass (mg) at the corrosion time and A_0 is the surface area (cm^2) of the sample contacted with molten salts.

Table 1
Impurity composition table of solar molten salt (nitro type).

| Impurity composition | Superior grade | First grade | Qualified product |
|--------------------------------|----------------|-------------|-------------------|
| Moisture wt% ≤ | 0.1 | 0.2 | 0.3 |
| Water insoluble wt% ≤ | 0.03 | 0.05 | 0.10 |
| Chloride(Cl^-)wt% ≤ | 0.01 | 0.03 | 0.05 |
| Fluoride(F^-)wt% ≤ | 0.003 | 0.004 | 0.005 |
| Barium ion precipitate | 0.08 | 0.10 | 0.12 |

Table 2

The ingredient of the studied stainless steels (wt%).

| Type of stainless steel | C | Mn | Si | P | S | Cr | Ni | Mo |
|-------------------------|--------|-------|-------|--------|--------|-----------|-----------|---------|
| 316L | ≤0.030 | ≤2.00 | ≤0.75 | ≤0.045 | ≤0.030 | 16.0–18.0 | 10.0–14.0 | 2.0–3.0 |

Based on the descaling data, the corrosion rate (CR) was estimated by Eq. (2).

$$CR \left(\frac{\text{mm}}{\text{y}} \right) = \frac{8.76 \times 10^4 \times \Delta m}{A_0 \times t \times \rho} \quad (2)$$

where t is the immersion time of the corrosion sample (h) and ρ is the density of stainless steel (g/cm^3): $\rho_{316L}=7.98 \text{ g}/\text{cm}^3$.

The standard deviation is introduced to reflect the discreteness of the results. The calculation formula of the standard deviation is shown in Eq. (3).

$$S = \sqrt{\frac{\sum_{i=1}^n (x_i - \bar{x})^2}{n-1}} \quad (3)$$

where x_i is the measured value of corrosion rate, \bar{x} is the average value of it, n is the sample numbers.

2.3. Microscopic observation

The microstructure and elemental analysis of the corrosion layers of stainless steel samples were characterized by scanning electron microscopy (SEM, Quanta 200, FEI) and energy dispersive X-ray spectrometry (EDS). All samples were observed by scanning electron microscope in 30 kV high vacuum modes. The element composition of stainless steel surface after corrosion was analyzed by EDS. The corrosion products were characterized by an X-ray diffractometer (XRD, D8-ADVANCE, Bruker). The data collection was carried out at room temperature, the XRD patterns were collected in 20 ranges from 10 to 80° and the acquisition rate is 1.2/min.

3. Results

3.1. The corrosion curve of stainless steel

Fig. 1 shows the corrosion rate of 316L stainless steel in quaternary

mixed molten salt with and without Cl^- varies with time. At the initial stage of corrosion, the corrosion rate of 316L stainless steel in quaternary mixed molten salt without Cl^- at 120 h is 0.0402 mm/y, while for quaternary mixed molten salt with Cl^- content of 0.01, 0.03 and 0.05 wt %, the corrosion rate of 316L stainless steel at 120 h is 0.0303, 0.0269 and 0.0267 mm/y respectively. 316L stainless steel has a relatively high corrosion rate in the quaternary mixed molten salt without Cl^- , which is higher than that with Cl^- . The reason of the higher corrosivity of quaternary mixed molten salt without Cl^- is perhaps due to the formation of hydroxyl ion from intercrystalline water of $\text{Ca}(\text{NO}_3)_2$. For quaternary mixed molten salt without Cl^- the hydroxyl ion perhaps can react with stainless steel directly, so its corrosion rate is high. While CaCl_2 can be formed when molten salt contains Cl^- , because CaCl_2 has high lattice energy, and CaCl_2 can react with hydroxyl ion to prevent the corrosion of stainless steel. In order to verify it, it is necessary to further analyze the corrosion products of stainless steel.

With the extension of corrosion time, the corrosivity of quaternary mixed molten salt without Cl^- continues to decrease, while it increases with time for quaternary mixed molten salt with Cl^- and reaches the maximum at 600 h. The reason is that the oxide scales of steel formed before 360 h were destroyed in an alkaline environment by Cl^- [12], so the corrosion rate of 316L in quaternary mixed molten salt with Cl^- increases with time. When corrosion time is longer than 600 h, the corrosivity of quaternary mixed molten salt with Cl^- begins to decrease. It may be that the stainless steel generates protective oxide scale in quaternary mixed molten salt with Cl^- , so the corrosion rate of 316L begins to decrease in the quaternary mixed molten salt with Cl^- for >600 h. Therefore, it is necessary to detect the microstructure of stainless steel after corrosion.

The results in Fig. 1 show that the corrosion rate of 316L stainless steel in quaternary mixed molten salt with Cl^- content of 0.03 wt% is the lowest due to the existence of Ca^{2+} . In order to confirm this conclusion, the corrosion dynamics law of stainless steel 316L in solar salt with and without additives (Cl^- or Cl^- and Ca^{2+}) was studied, as shown in Fig. 2. The results show that the corrosion rate of 316L stainless steel in solar salt with and without additives (Cl^- or Cl^- and Ca^{2+}) decreases with the increase in corrosion time. Also, the corrosivity of molten salt without Cl^- is maximum, while it is minimum when molten salt contains the Cl^-

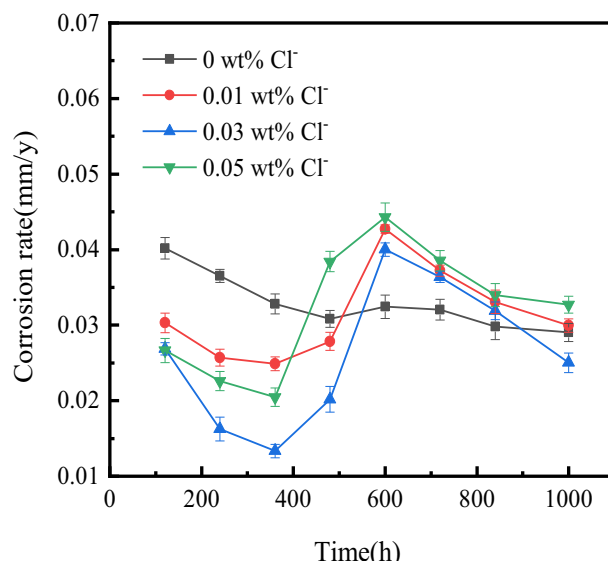


Fig. 1. Corrosion rate curve of 316L stainless steel in quaternary mixed molten salt with and without Cl^- at 565 °C.

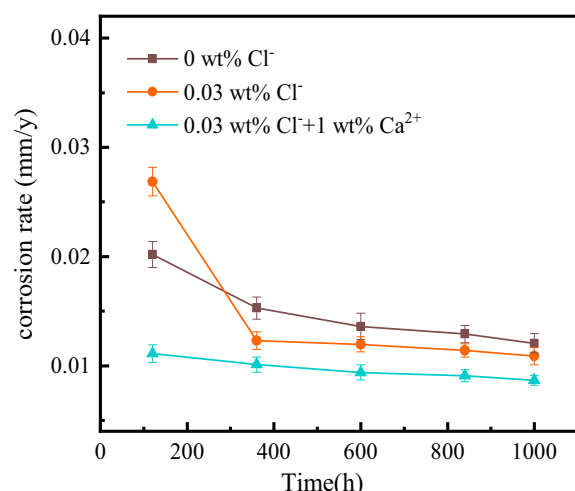


Fig. 2. Corrosion rate curve of 316L stainless steel in solar salt with and without additives (Cl^- or Cl^- and Ca^{2+}) at 565 °C.

and Ca^{2+} . It can be seen that the introduction of Cl^- and Ca^{2+} can decrease corrosion rate of 316L stainless steel. The same results were gotten as that of quaternary mixed molten salt in Fig. 1.

The comparison results of the corrosion rate of 316L stainless steel at 1000 h in two molten nitrate salts with and without Cl^- are shown in Fig. 3. It can be seen that the corrosion rate of 316L stainless steel in two molten nitrate salts with low Cl^- content is relatively low, which $<0.0350 \text{ mm/y}$. However, the corrosivity of quaternary mixed molten salt with and without Cl^- is higher than that of solar salt for the existence of intercrystalline water in $\text{Ca}(\text{NO}_3)_2$. Especially, when Ca^{2+} is introduced, the corrosion of molten salt with Cl^- can be decreased. For example, when solar salt with Cl^- content of 0.03 wt%, its corrosion rate to 316L stainless steel can be decreased from 0.0121 to 0.0087 mm/y with the addition of Ca^{2+} , while it is decreased from 0.0290 to 0.0250 mm/y for the quaternary mixed molten salt with Cl^- content of 0.03 wt %. It can be seen that in the real application the low cost of first grade molten salt with Cl^- can be chosen for thermal energy storage when adding small content of Ca^{2+} .

3.2. Cross-section detection

In order to further observe the distribution and morphology of the elements of the corrosion layer and stainless steel matrix, the cross sections of stainless steel samples were analyzed by SEM and EDS.

Fig. 4 shows that SEM images and EDX mapping of the cross-section of 316L stainless steel in quaternary mixed molten salt with and without Cl^- for 1000 h corrosion test at 565 °C. It can be seen that the cross-section of 316L stainless steel forms a relatively dense corrosion layer in quaternary mixed molten salt when Cl^- content is $\leq 0.03 \text{ wt\%}$, as shown in Fig. 4a, b and c. However, the corrosion layer of stainless steel peels off when Cl^- content is 0.05 wt%, as shown in Fig. 4d, which is a negative impact on the protection of stainless steel corrosion layer to the matrix. The reason may be that the addition of Cl^- causes the formation of metal chloride in the corrosion layer, and the metal chloride has a high volatility, which makes the corrosion layer peel off [8,9].

The thickness of corrosion layer of 316L stainless steel in quaternary mixed molten salt with and without Cl^- for 1000 h can also be obtained from Fig. 4. It is about 31.8 μm (as shown in Fig. 4a) for quaternary mixed molten salt without Cl^- , and it is about 32.7, 30.9 and 33.3 μm when the quaternary mixed molten salt with the Cl^- content of 0.01, 0.03 and 0.05 wt%, respectively, as shown in Fig. 4b, c and d. Comparing these results, it can be found that the corrosion layer thickness of stainless steel in the quaternary mixed molten salt with Cl^-

content of 0.03 wt% is the lowest (30.9 μm), which is consistent with the corrosion rate obtained in the 1000 h (as shown in Fig. 3).

Fig. 4 also shows the EDX mapping of the cross section of 316L stainless steel in quaternary mixed molten salt with and without Cl^- . It can be observed that the O, Fe, Cr, Ni and Ca elements exist in the corrosion layer of 316L stainless steel. The corrosion layer of 316L stainless steel forms the Calcium (Ca) rich oxide layer when quaternary mixed molten salt with Cl^- . While a small amount of Ca was found in the corrosion layer of 316L stainless steel when quaternary mixed molten salt without Cl^- . This indicates that the existence of Cl^- in molten salt leads to the formation of Ca rich oxide layer in the corrosion layer of stainless steel. By comparing Fig. 4b, c and d, it can be found that the corrosion layer of 316L stainless steel forms a denser Ca rich oxide layer in quaternary mixed molten salt with Cl^- content of 0.03 wt%.

Fig. 5 shows that SEM images and EDX mapping of the cross-section of 316L stainless steel in solar salt with and without additives (Cl^- or Cl^- and Ca^{2+}) for 1000 h corrosion test at 565 °C. It can be seen that the cross-section of 316L stainless steel forms a relatively dense corrosion layer in solar salt with and without additives (Cl^- or Cl^- and Ca^{2+}), as shown in Fig. 5a, b and c. The thickness of corrosion layer of 316L stainless steel in solar salt with and without additives (Cl^- or Cl^- and Ca^{2+}) for 1000 h can also be obtained from Fig. 5. For solar salt without and with Cl^- , the thickness of corrosion layer of 316L stainless steel is about 27.2 and 26.9 μm , respectively, as shown in Fig. 5a and b. However, when Ca^{2+} is introduced, the corrosion layer thickness of 316L stainless steel in solar salt with Cl^- and Ca^{2+} is the lowest, which is about 26.3 μm (as shown in Fig. 5c). This indicates that the addition of Cl^- and Ca^{2+} can inhibit the corrosion of stainless steel in solar salt.

It can be found that the O, Fe, Cr and Ni elements exist in the corrosion layer of 316L stainless steel, as shown in Fig. 5. At the same time, the Ca element was also found in the corrosion layer of 316L stainless steel in solar salt with Cl^- and Ca^{2+} , and it also formed a Ca rich oxide layer. Comparing with Figs. 4 and 5, it can be found that the formation condition of Ca rich oxide layer may be the presence of both Cl^- and Ca^{2+} in molten salts.

3.3. Surface morphology analysis and structure characterization

In order to appraise the effect of Cl^- on the morphology of 316L stainless steel, the surface microstructure of 316L stainless steel was observed and analyzed by SEM and EDS.

Fig. 6 shows the SEM images and corresponding zone EDS of 316L surface in quaternary mixed molten salt with and without Cl^- . It can be seen that a dense oxide scale was formed on the surface of 316L in quaternary mixed molten salt without Cl^- , but a small amount of oxide scales peeling can also be found, as shown in Fig. 6a. Such similar oxide scales peeling phenomenon has also been mentioned in previous studies [13]. In the zone A of Fig. 6a, the main elements of oxide scale are O and Fe, and small amounts of Ca, Ni and Cr (as shown in Fig. 6b).

However, when the Cl^- content in quaternary mixed molten salt is 0.01 wt%, a small number of blocky-shaped particles were formed on the surface of 316L stainless steel, as shown in Fig. 6c. The blocky-shaped particles are also found on the surface of 316L stainless steel in quaternary mixed molten salt with Cl^- content of 0.03 wt% and 0.05 wt %. The blocky-shaped particles contain not only Fe and O elements but also Ca (as shown in Fig. 6d, f and h), which indicates that the blocky-shaped particles are oxides of calcium and iron. Comparing with Figs. 4 and 6, it can be inferred that the Ca rich oxide layer of 316L stainless steel is composed of blocky-shaped particles. In the quaternary mixed molten salt with Cl^- content of 0.05 wt%, not only blocky-shaped particles but also many cracks were found on the surface of 316L stainless steel, as shown in Fig. 6g. Because the corrosion layer of stainless steel cracks and peel off (as shown in Fig. 4d), the corrosion rate of stainless steel in quaternary mixed molten salt with Cl^- content of 0.05 wt% for 1000 h is higher than that of the other three molten salts.

Fig. 7 shows that SEM images and corresponding zone EDS the

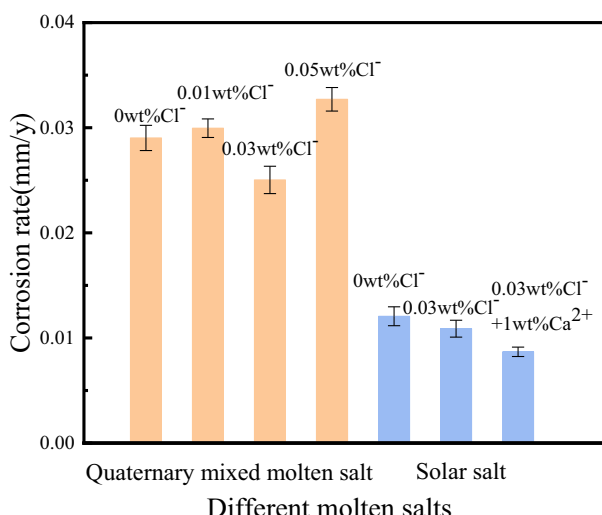


Fig. 3. The comparison results of the corrosion rate of 316L stainless steel in different molten salts at 1000 h.

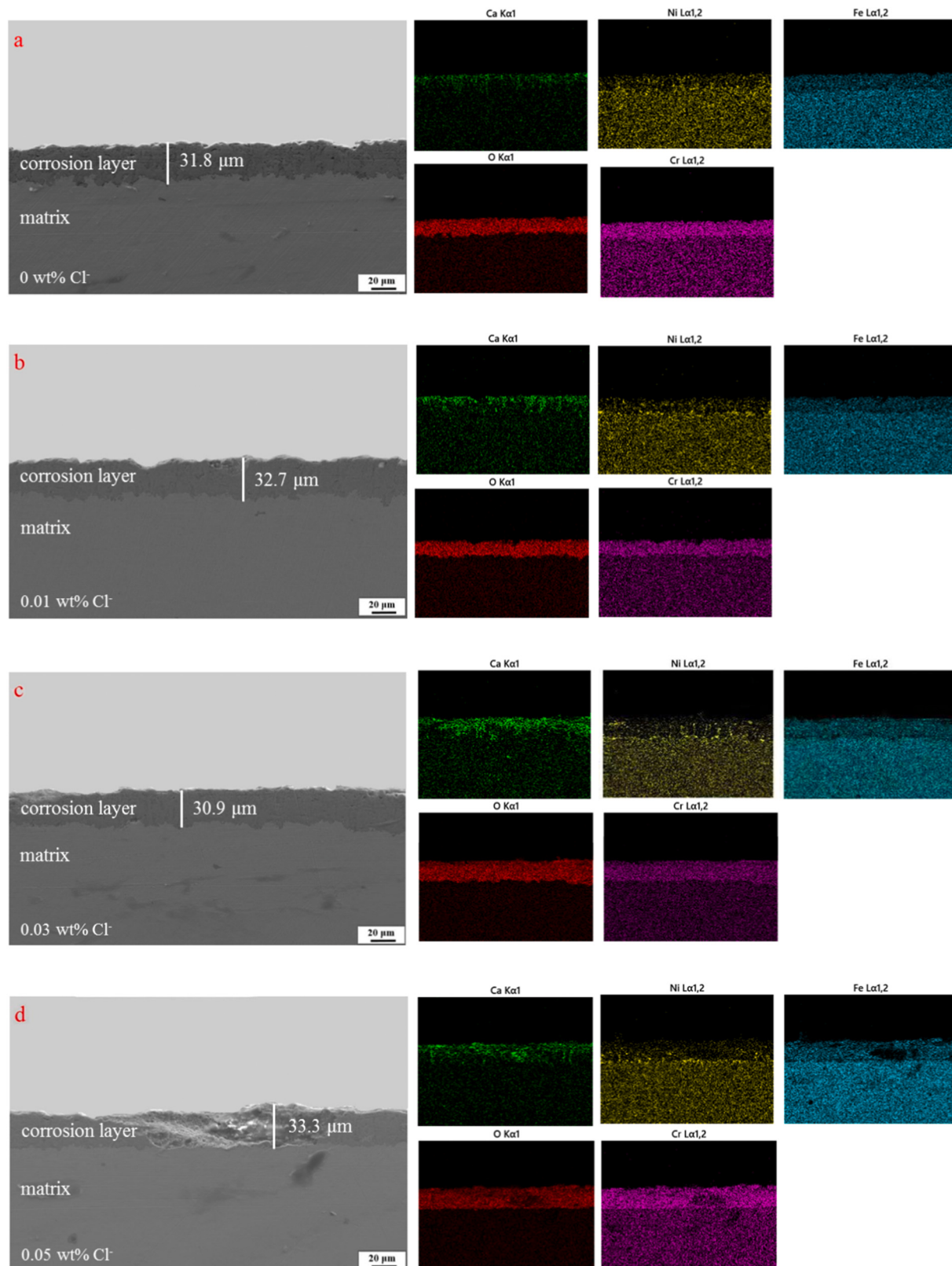


Fig. 4. SEM images and EDX mapping of the cross-section of 316L stainless steel in quaternary mixed molten salt with and without Cl^- for 1000 h corrosion test at 565 °C.

surface of 316L stainless steel in solar salt with and without additives (Cl^- or Cl^- and Ca^{2+}) for 1000 h corrosion test at 565 °C. The dense oxide scales can also be found on the surface of 316L stainless steel in solar salt with and without Cl^- , as shown in Fig. 7a and c. And the main

elements of oxide scale in the corresponding zone are O and Fe, and small amounts of Ni and Cr (as shown in Fig. 7b and d). The blocky-shaped particles are also found on the surface of 316L stainless steel in solar salt with Cl^- and Ca^{2+} , and its element composition is Ca, Fe and O.

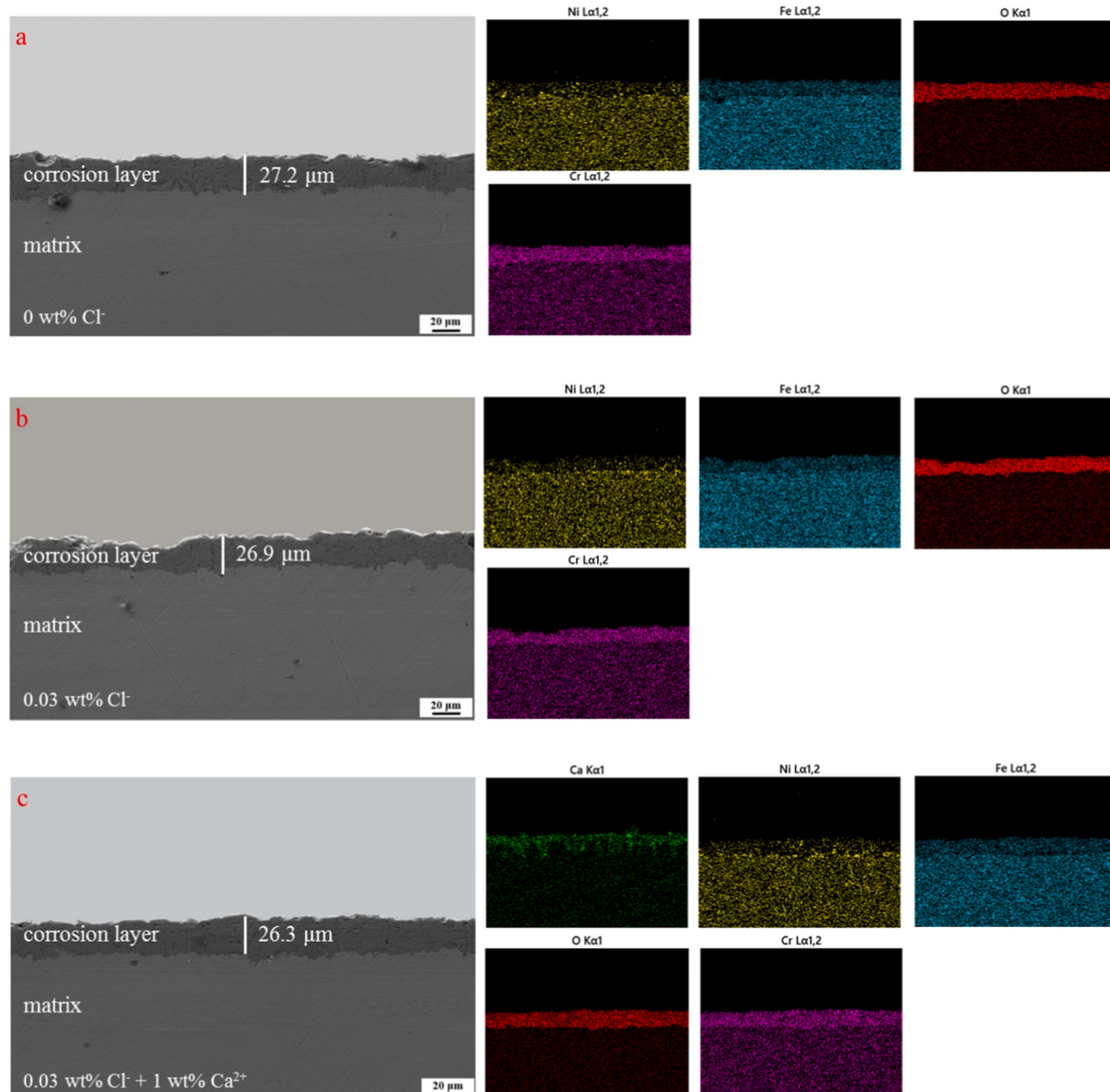


Fig. 5. SEM images and EDX mapping of the cross section of 316L stainless steel in solar salt with and without additives (Cl^- or Cl^- and Ca^{2+}) for 1000 h corrosion test at 565 °C.

It can be inferred that the Ca rich oxide layer composed of blocky-shaped particles provides protection for stainless steel and reduces the corrosion rate of stainless steel in molten salt.

3.4. Corrosion products

The above results show that 316L stainless steel has different corrosion dynamics law and microstructure in molten salt with and without Cl^- . In order to further study the effect of Cl^- on the corrosion process of molten salt, it is necessary to analyze corrosion products of stainless steel in molten salt with and without Cl^- by XRD analysis.

Fig. 8 shows that XRD patterns of 316L stainless steel in quaternary mixed molten salt with and without Cl^- for 360 h corrosion test at 565 °C. The results show that the main phase such as Fe_2O_3 , Fe_3O_4 , FeCr_2O_4 and Fe_3Ni_2 can be obtained in the corrosion layer of 316L for quaternary mixed molten salt with and without Cl^- . In previous studies [14–17], it was found that Fe_2O_3 and Fe_3O_4 were the main corrosion products of stainless steel in contact with molten salt, according to reactions (4) and (5):



In addition, previous studies [17] found that Fe and Cr elements (as shown in Table 2) in 316L stainless steel form FeCr_2O_4 after corrosion, which is a dense spinel structure, according to reaction (6):



However, a small amount of $\text{Ca}(\text{OH})_2$ was observed in the corrosion layer of 316L in the quaternary mixed molten salt with Cl^- , but not in quaternary mixed molten salt without Cl^- . This indicates that when molten salt contains Cl^- , $\text{Ca}(\text{OH})_2$ can be formed by CaCl_2 and hydroxyl ion reaction, which consumes part of the hydroxide ion in the molten salt. So, the corrosion rate of stainless steel in the quaternary mixed molten salt with Cl^- is lower than that in the quaternary mixed molten salt without Cl^- before 360 h (as shown in Fig. 1).

Fig. 9 shows that XRD patterns of 316L stainless steel in solar salt with and without additives (Cl^- or Cl^- and Ca^{2+}) for 360 h corrosion test

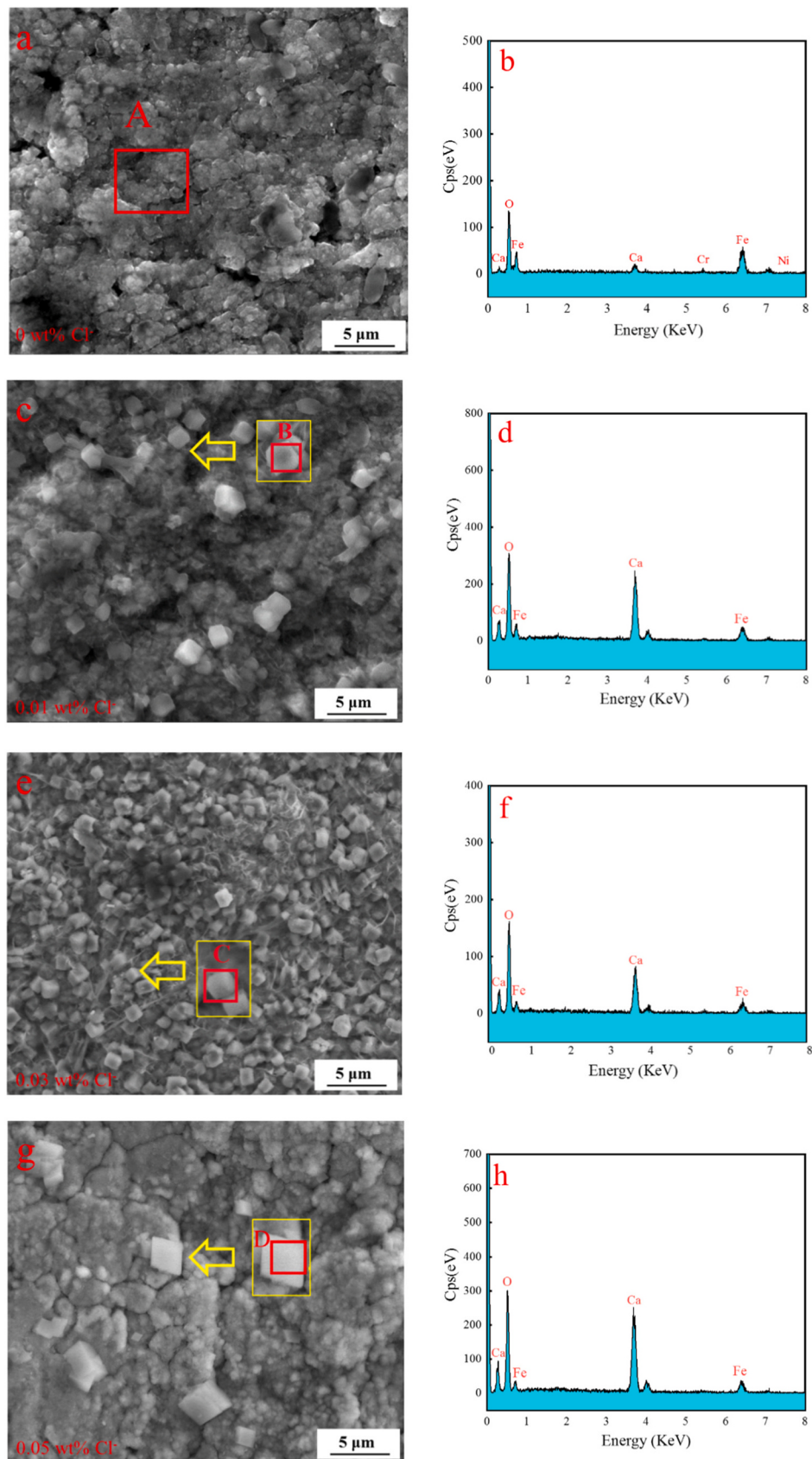


Fig. 6. SEM images and corresponding zone EDS the surface of 316L stainless steel in quaternary mixed molten salt with and without Cl^- for 1000 h corrosion test at 565 °C.

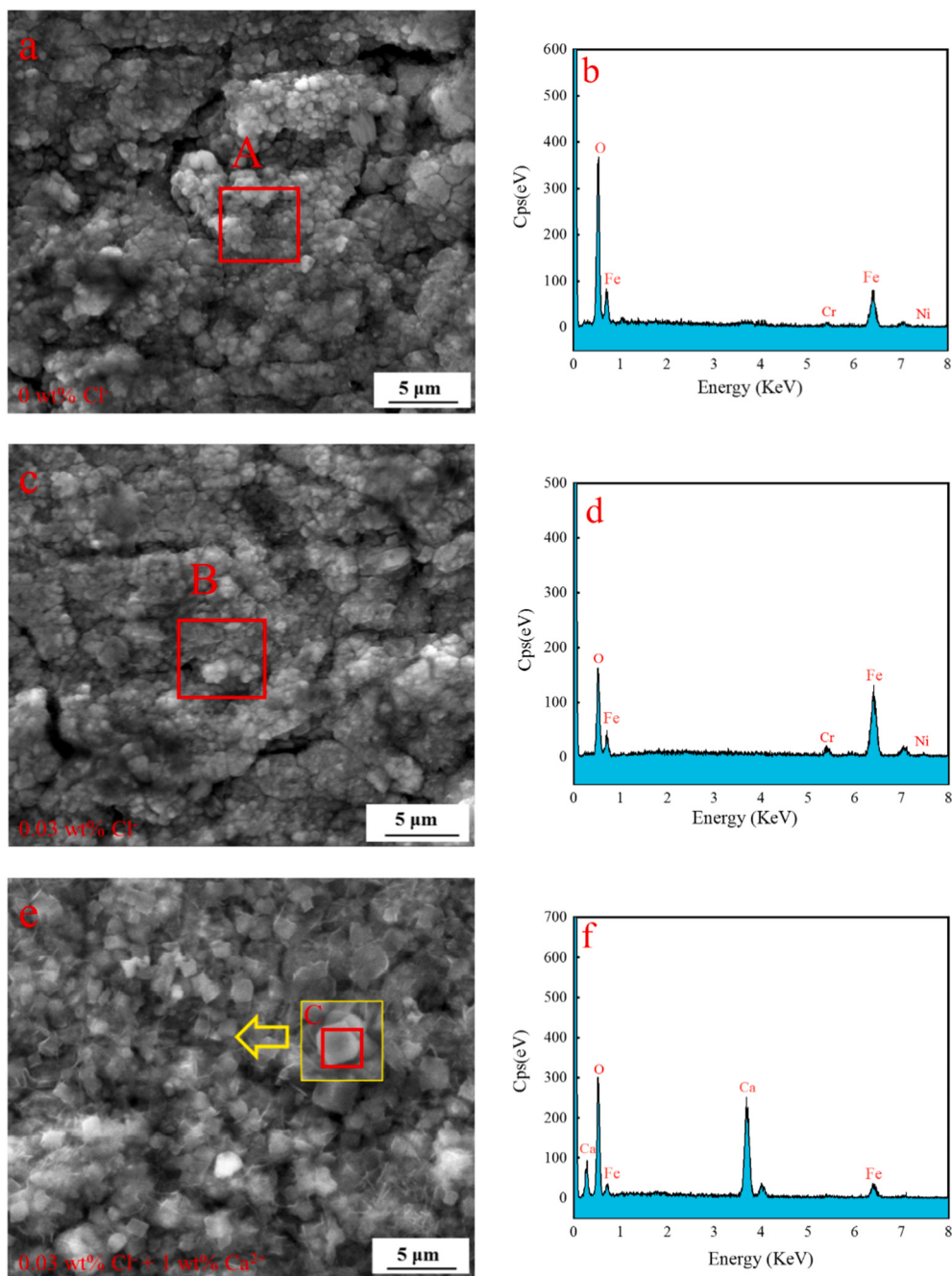


Fig. 7. SEM images and corresponding zone EDS the surface of 316L stainless steel in solar salt with and without additives (Cl^- or Cl^- and Ca^{2+}) for 1000 h corrosion test at 565 °C.

at 565 °C. It can be seen that Fe_2O_3 , Fe_3O_4 , FeCr_2O_4 and Fe_3Ni_2 also were found in the corrosion layer of 316L stainless steel for solar salt with and additives (Cl^- or Cl^- and Ca^{2+}). Comparing Figs. 8 and 9, it can be found that the diffraction peak of corrosion products of stainless steel in solar salt is low, which verifies that the corrosion rate of stainless steel in solar salt is lower than that of quaternary salt (as shown in Fig. 3).

Fig. 10 shows that the XRD patterns of 316L stainless steel in quaternary mixed molten salt with and without Cl^- for 1000 h corrosion test at 565 °C. It can be seen that similar products (such as Fe_2O_3 , Fe_3O_4 , FeCr_2O_4 and Fe_3Ni_2) were found in the corrosion layer of 316L stainless steel in quaternary mixed molten salt with and without Cl^- for 1000 h. However, there are some diffraction peaks of CaFeO_4 in the corrosion layer for quaternary mixed molten salt with Cl^- , but there is no diffraction peak of CaFeO_4 in the corrosion layer for quaternary mixed

molten salt without Cl^- . From the above SEM and EDS test results of 316L, it can be inferred that the blocky-shaped particles composed of Ca, Fe and O are CaFeO_4 .

Fig. 11 shows that XRD patterns of 316L stainless steel in solar salt with and without additives (Cl^- or Cl^- and Ca^{2+}) for 1000 h corrosion test at 565 °C. Similarly, the main corrosion products (such as Fe_2O_3 , Fe_3O_4 , FeCr_2O_4 and Fe_3Ni_2) were also found in the corrosion layer of 316L for solar salt with and without additives (Cl^- or Cl^- and Ca^{2+}), as shown in Fig. 11. Moreover, CaFeO_4 also found in the corrosion layer of 316L stainless steel for solar salt with Cl^- and Ca^{2+} . Based on the above, it is reasonable that there is CaFeO_4 in the corrosion layer of 316L stainless steel, which can inhibit corrosion in molten salt.

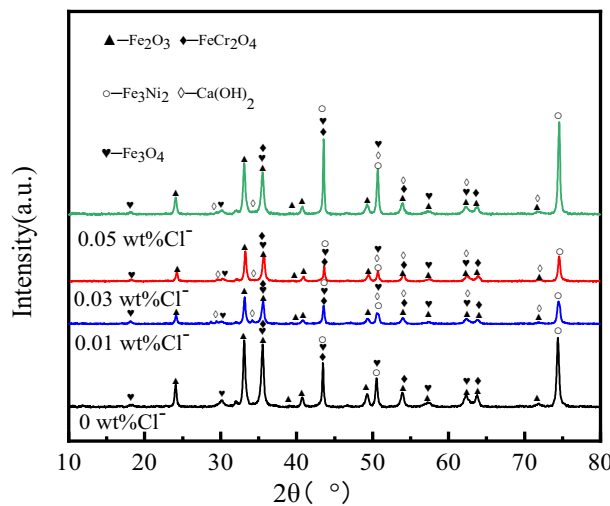


Fig. 8. XRD patterns of 316L stainless steel in quaternary mixed molten salt with and without Cl^- for 360 h corrosion test at 565 °C.

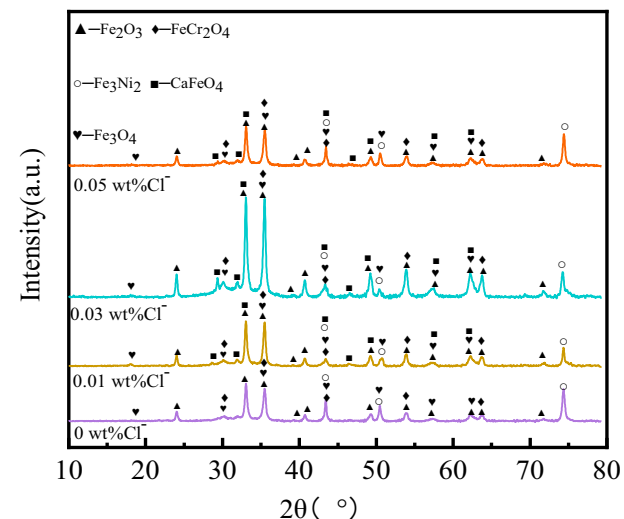


Fig. 10. XRD patterns of 316L stainless steel in quaternary mixed molten salt with and without Cl^- for 1000 h corrosion test at 565 °C.

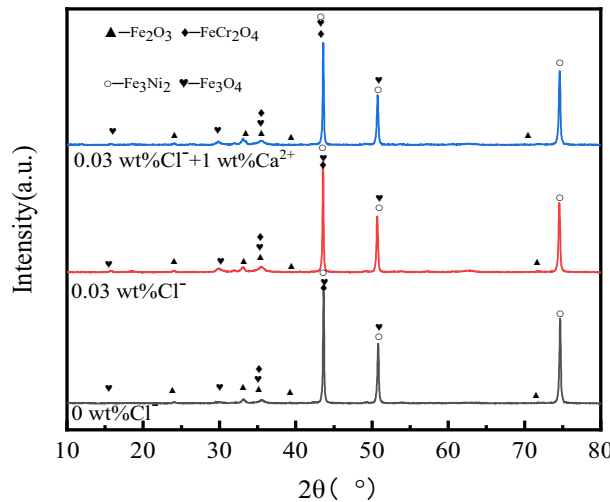


Fig. 9. XRD patterns of 316L stainless steel in solar salt with and without additives (Cl^- or Cl^- and Ca^{2+}) for 360 h corrosion test at 565 °C.

3.5. Effect of Cl^- on corrosion process of stainless steel in molten salt

Based on the above results, the effect of Cl^- on corrosion process of stainless steel in molten salt are illustrated in Fig. 12. When the molten salt contains Cl^- , Cl^- may combine with K, Na and Ca to form chloride. Compared with KCl and NaCl , CaCl_2 has larger lattice energy. In general, the higher the lattice energy, which indicates that the crystal is more stable. Therefore, it is more possible for Cl^- to combine with Ca^{2+} ion to form CaCl_2 .

In the previous literature [18], it was mentioned that H_2O is one of the important factors that affect the corrosion rate of stainless steel in molten salt, according to reaction (7):



In addition, the quaternary mixed molten salt may contain more hydroxyl ion than solar salt for the existence of intercrystalline water in $\text{Ca}(\text{NO}_3)_2$. A small amount of $\text{Ca}(\text{OH})_2$ was found on the surface of the stainless steel sample in the quaternary mixed molten salt with Cl^- for 360 h (as shown in Fig. 8). After the combination of Cl^- and Ca^{2+} , it reacts with the hydroxyl ion generated in reaction (7) to generate $\text{Ca}(\text{OH})_2$, according to reaction (8):

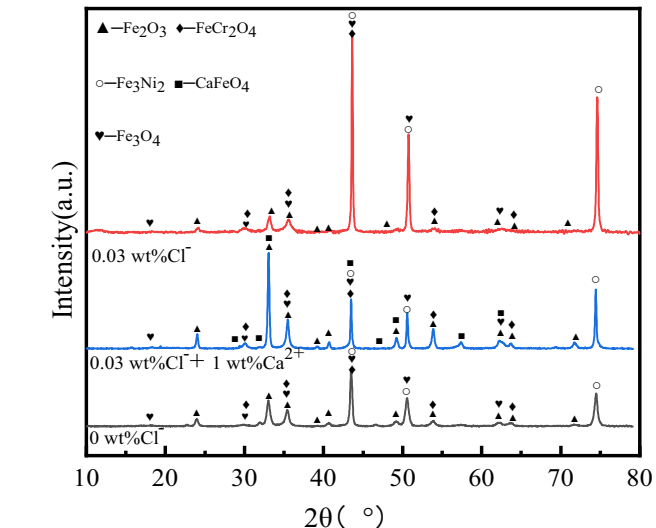


Fig. 11. XRD patterns of 316L stainless steel in solar salt with and without additives (Cl^- or Cl^- and Ca^{2+}) for 1000 h corrosion test at 565 °C.



For solar salt with Cl^- and Ca^{2+} , $\text{Ca}(\text{OH})_2$ was not detected in the corrosion layer, which may be due to the small content of Ca^{2+} added to the solar salt with Cl^- and Ca^{2+} . For quaternary mixed molten salt without Cl^- , no $\text{Ca}(\text{OH})_2$ was found in the corrosion layer of 316L stainless steel, which indicates that $\text{Ca}(\text{OH})_2$ can only be formed under the action of Cl^- and Ca^{2+} .

Previous studies [12] have found that the oxide scales of steel were destroyed in an alkaline environment with Cl^- , which increases the corrosion rate of steel. This explains the reason why the corrosion rate of 316L stainless steel increases after 360 h in quaternary mixed molten salt with Cl^- (as described by the red arrow in Fig. 12a). While the corrosion rate of 316L stainless steel does not increase in solar salt with Cl^- and Ca^{2+} after 360 h, which may be due to the fact that solar salt has less hydroxyl ions. Therefore, the oxide scale of stainless steel in solar salt was less destroyed from Cl^- and OH^- .

Moreover, due to the presence of Cl^- in molten salt, it has been mentioned in previous studies that the acceleration of stainless steel

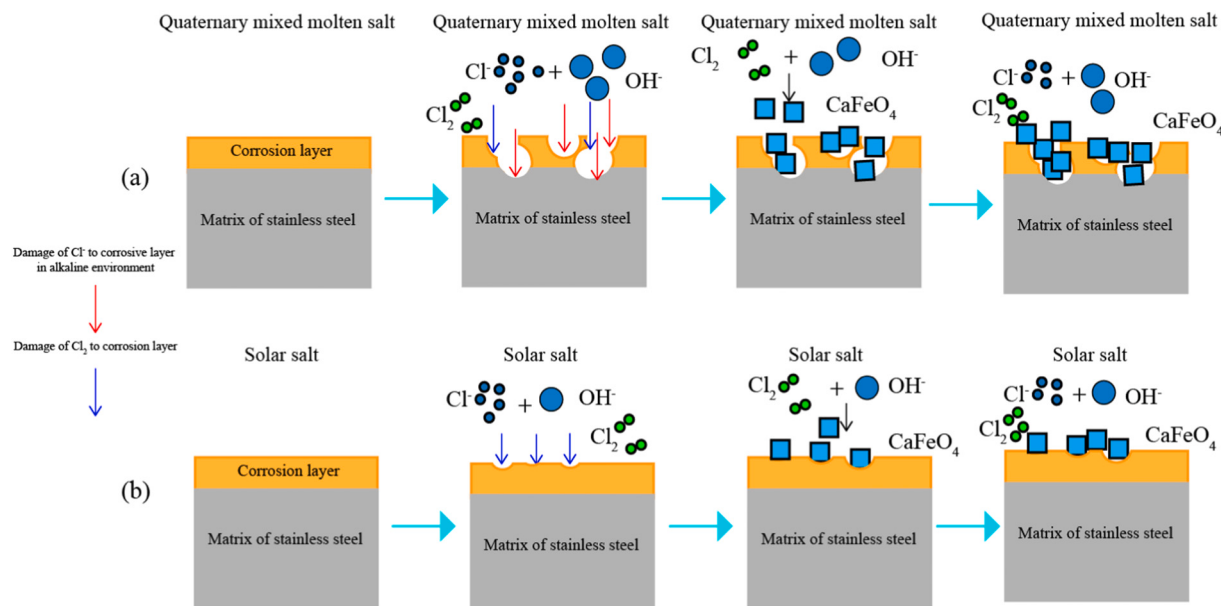
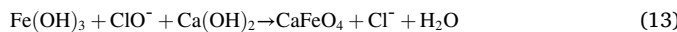


Fig. 12. Schematic representation of the effect of Cl^- on corrosion process of stainless steel in molten salt.

corrosion caused by Cl^- in molten salt is mainly based on the following reactions [18,19]:



FeCl_2 is easy to volatilize and has no good protective effect on stainless steel matrix (as described by the blue arrow in Fig. 12). In this study, the corrosion layer of 316L stainless steel peeled off in quaternary mixed molten salt with Cl^- content of 0.05 wt% (as shown in Fig. 4d), while the corrosion layer of stainless steel did not peel off in other molten salts with Cl^- (as shown in Figs. 4 and 5). It can be concluded that the corrosion layer of stainless steel has no negative effect on the protection of the matrix in molten salts with Cl^- of 0.01 % and 0.03 wt%. Besides, the Cl_2 in the above reactions reacts with hydroxide ions to form CaFeO_4 under certain conditions [20], according to reactions (12) and (13):



As shown in Fig. 12, CaFeO_4 in the corrosion layer can provide protection for the stainless steel matrix. For the quaternary mixed molten salt with Cl^- , the corrosion rate of 316L stainless steel decreases when the corrosion time exceeds 600 h, which indicates that the corrosion rate of 316L stainless steel decreases after 600 h due to the presence of CaFeO_4 . Moreover, the corrosion rate of 316L stainless steel was reduced by adding Cl^- and Ca^{2+} to the solar salt, which is also because CaFeO_4 in the corrosion layer can provide protection for the stainless steel matrix (as shown in Fig. 12b).

4. Conclusions

The corrosion behavior of 316L stainless steel at 565 °C in two molten nitrate salts with and without Cl^- for 1000 h was studied. The main results are summarized as follows:

- (1) The corrosion rate of 316L stainless steel in quaternary mixed molten salt with low Cl^- content (0.01–0.05 wt%) is relatively low at 1000 h, which <0.0350 mm/y. And the corrosion rate of 316L stainless steel in quaternary mixed molten salt with Cl^- content of 0.03 wt% is the lowest, which is 0.0250 mm/y.
- (2) The addition of Cl^- and Ca^{2+} in molten salt can reduce the corrosion rate of stainless steel significantly with the mixed nitrate. The corrosion reduction of stainless steel is mainly from the formation of Ca rich oxide layers composed of the blocky-shaped particles in the corrosion layer, which can inhibit corrosion.
- (3) The main corrosion products of 316L stainless steels were Fe_2O_3 , Fe_3O_4 and FeCr_2O_4 in both quaternary mixed molten salt and solar salt. Moreover, the CaFeO_4 was found in the corrosion layer of 316L stainless steel for the molten salt with Cl^- and Ca^{2+} .

CRediT authorship contribution statement

Qi Gao: Methodology, Formal analysis, Investigation, Writing – original draft, Validation. **Yuanwei Lu:** Conceptualization, Resources, Writing – review & editing, Funding acquisition. **Yanchun Yang:** Formal analysis, Investigation. **Yuting Wu:** Resources, Writing – review & editing, Funding acquisition. **Canccan Zhang:** Formal analysis, Writing – review & editing. **Zhansheng Fan:** Investigation, Formal analysis.

Declaration of competing interest

The authors declare that they have no known competing financial interests or personal relationships that could have appeared to influence the work reported in this paper.

Data availability

No data was used for the research described in the article.

Acknowledgements

This work is supported by the National Natural Science Foundation of China (No. 52076006) and Inner Mongolia Science and Technology Major Project (No. 2021ZD0036).

References

- [1] Y. Grosu, O. Bondarchuk, A. Faik, The effect of humidity, impurities and initial state on the corrosion of carbon and stainless steels in molten HitecXL salt for CSP application, *Sol. Energy Mater. Sol. Cells* 174 (2018) 34–41.
- [2] W. Yuting, R. Nan, M. Chongfang, Research and application of molten salts for sensible heat storage, *Energy Storage Sci. Technology* 2 (2013) 586–592.
- [3] M. Walczak, F. Pineda, A.G. Fernandez, C. Mata-Torres, R.A. Escobar, Materials corrosion for thermal energy storage systems in concentrated solar power plants, *Renew. Sust. Energ. Rev.* 86 (2018) 22–44.
- [4] Y. Xiao, L. Ding, W. Liao, Y. Zhang, H. Jie, X. Ding, Corrosion resistances of 304,316L and 321 austenite stainless steel in nitrate molten salt, *Mater. Rev.* 30 (2016) 217–219.
- [5] A. Kruizenga, D. Gill, Corrosion of iron stainless steels in molten nitrate salt, *Energy Procedia* 49 (2014) 878–887.
- [6] A. Gomes, M. Navas, N. Uranga, T. Paiva, I. Figueira, T.C. Diamantino, High-temperature corrosion performance of austenitic stainless steels type AISI 316L and AISI 321H, *Sol. Energy* 177 (2019) 408–419.
- [7] GB/T. 36376, Solar Molten Salt (Nitro Type), 2018.
- [8] F. Javier, C. Ruiz, C. Prieto, V. Madina, Materials selection for thermal energy storage systems in parabolic trough collector solar facilities using high chloride content nitrate salts, *Sol. Energy Mater. Sol. Cells* 163 (2017) 134–147.
- [9] K. Federsel, J. Wortmann, M. Ladenberger, High-temperature and corrosion behavior of nitrate nitrite molten salt mixtures regarding their application in concentrating solar power plants, *Energy Procedia* 69 (2015) 618–625.
- [10] L.L. Zou, X. Chen, Y.T. Wu, X. Wang, C.F. Ma, Experimental study of thermophysical properties and thermal stability of quaternary nitrate molten salts for thermal energy storage, *Sol. Energy Mater. Sol. Cells* 190 (2019) 12–19.
- [11] Z. Sun, L. Su, G. Xianyang, Influences of impurity cl on the thermal performance of solar salt for thermal energy storage, *Sol. Energy* 216 (2021) 90–95.
- [12] M. Wu, J.J. Shi, Beneficial and detrimental impacts of molybdate on corrosion resistance of steels in alkaline concrete pore solution with high chloride contamination, *Corros. Sci.* 183 (2021), 109326.
- [13] W. Wang, B. Guan, X. Li, Corrosion behavior and mechanism of austenitic stainless steels in a new quaternary molten salt for concentrating solar power, *Sol. Energy Mater. Sol. Cells* 194 (2019) 36–46.
- [14] A.G. Fernandez, H. Galleguillos, F.J. Perez, Thermal influence in corrosion properties of Chilean solar nitrates, *Sol. Energy* 109 (2014) 125–134.
- [15] W.J. Cheng, D.J. Chen, C.J. Wang, High-temperature corrosion of Cr-Mo steel in molten LiNO₃-NaNO₃-KNO₃ eutectic salt for thermal energy storage, *Sol. Energy Mater. Sol. Cells* 132 (2015) 563–569.
- [16] Z. Xiaoming, Z. Cancan, W. Yuting, Experimental research of high temperature dynamic corrosion characteristic of stainless steels in nitrate eutectic molten salt, *Sol. Energy* 209 (2020) 618–627.
- [17] L. Heng, W. Xiaowei, Y. Xuzhong, Yang Xinyu, T. Jianqun, G. Jianming, Corrosion and electrochemical investigations for stainless steels in molten solar salt: the influence of chloride impurity, *J. Energy Storage* 39 (2021), 102675.
- [18] A.G. Fernandez, L.F. Cabeza, Molten salt corrosion mechanisms of nitrate based thermal energy storage materials for concentrated solar power plants: a review, *Sol. Energy Mater. Sol. Cells* 194 (2019) 160–165.
- [19] H.J. Grabke, E. Reese, M. Spiegel, The effects of chlorides, hydrogen chloride, and sulfur dioxide in the oxidation of steels below deposits, *Corros. Sci.* 37 (1995) 1023–1043.
- [20] A.H. Alshahri, L. Fortunato, N. Ghaffour, Controlling harmful algal blooms (HABs) by coagulation-flocculation-sedimentation using liquid ferrate and clay, *Chemosphere* 68 (2021), 129676.